

Extraction Heights for STIS Echelle Spectra

Claus Leitherer and Ralph Bohlin
March 1998

ABSTRACT

The optimum extraction height (h) for STIS echelle spectra of 7 pixels maximizes the signal-to-noise for all modes and encompasses more than 98% of the target flux. Reducing h from 11 to 7 pixels reduces the error in the background correction by 40% at Lyman- α . This 7 pixel extraction height perpendicular to the dispersion should be the default for echelle extractions in the pipeline.

1. Introduction

The trade-offs among different considerations for optimum extraction heights for first-order STIS gratings are discussed in ISR STIS 97-13 (Leitherer & Bohlin 1997). The preferred slit heights for first-order modes are a compromise between spectral purity, signal-to-noise, and photometric precision. Two additional issues must be addressed when extracting STIS echelle spectra. First, individual orders have a finite spatial separation, imposing a mode and order dependent upper limit on the maximum extraction height. Second, the E140M and E140H modes suffer from significant scattered light, whose contribution to the extracted spectrum increases with increasing extraction height.

In this ISR we determine the optimum echelle extraction height and recommend the implementation of this height in the calibration pipeline.

2. Observations and Data Reduction

The data which define the optimum extraction height are summarized in Table 1. The observations in this table were taken as part of several SMOV and Cycle 7 calibration programs. The target was a spectrophotometric standard star in all cases. The available data are sufficient to characterize all four STIS echelle modes (E140M, E140H, E230M, E230H) over the entire wavelength region of interest.

Table 1. Observation details

Rootname	Mode	Aperture	Wavelength	Detector	Target	Prop ID
O3ZX02X5Q	E140M	0.2X0.2	1425	FUV-MAMA	BD+28D4211	7096
O3ZX02XAQ	E230M	0.2X0.2	1978	NUV-MAMA	BD+28D4211	7096
O3ZX02XEQ	E230M	0.2X0.2	2707	NUV-MAMA	BD+28D4211	7096
O3ZX02XGQ	E230M	0.2X0.2	2707	NUV-MAMA	BD+28D4211	7096
O3ZX10DAQ	E140H	0.2X0.2	1416	FUV-MAMA	BD+75D325	7096
O3ZX10DEQ	E230H	0.2X0.2	2513	NUV-MAMA	BD+75D325	7096
O45930010	E140H	0.2X0.2	1416	FUV-MAMA	BD+28D4211	7673
O45930020	E230H	0.2X0.2	2263	NUV-MAMA	BD+28D4211	7673
O45930030	E140M	0.2X0.2	1425	FUV-MAMA	BD+28D4211	7673
O45930040	E230M	0.2X0.2	1978	NUV-MAMA	BD+28D4211	7673
O45930050	E230M	0.2X0.2	2707	NUV-MAMA	BD+28D4211	7673
O47S01020	E140H	0.2X0.09	1307	FUV-MAMA	BD+33D2642	7104
O47S01030	E140H	0.2X0.09	1307	FUV-MAMA	BD+33D2642	7104
O4DD05020	E230H	0.2X0.2	2013	NUV-MAMA	BD+75D325	7657
O4DD05030	E230H	0.2X0.2	1763	NUV-MAMA	BD+75D325	7657
O4DD05040	E230H	0.2X0.2	2263	NUV-MAMA	BD+75D325	7657
O4DD05050	E230H	0.2X0.2	2762	NUV-MAMA	BD+75D325	7657
O4DD05060	E230H	0.2X0.2	3012	NUV-MAMA	BD+75D325	7657
O4DD05070	E140H	0.2X0.2	1234	FUV-MAMA	BD+75D325	7657
O4DD05080	E140H	0.2X0.2	1598	FUV-MAMA	BD+75D325	7657

After sequentially performing the standard reduction steps to the raw data up to the flatfield corrections, the two-dimensional images are geometrically corrected. The one-dimensional spectra are extracted and wavelength calibrated from 1024 x 1024 images using extraction heights of 3, 5, 7, 9, 11, 15, and 21 pixels. The corresponding background data are the inter-order count rates from the two-dimensional images after filtering and fitting with 3rd-order polynomials for each order. The background spectra are subtracted from the gross science spectra to produce the net spectra for each observation, order, and extraction height.

There is no optimal extraction algorithm that could satisfy every observer's needs. Even for a point source, the optimal height of an extraction aperture depends on the PSF width, the target flux relative to the background, and the trade-off between flux conservation, maximum signal-to-noise, and spectral purity. As in the case for the first-order

gratings, a simple, robust extraction algorithm with few parameters is adequate for the scientific analysis of most point source data.

3. Spectral Purity of STIS Echelle Observations

As with most other echelle spectrographs, STIS echelle data are affected by spectral order overlap at the shortest wavelengths where adjacent spectral orders are not well separated due to the degraded PSF in the UV. Some fraction of the spectral signal from the next higher (or lower) order is included in the background, introducing spectral impurity. In addition, the echelle data suffer from significant scattered light, especially at the shortest wavelengths.

Figure 1 highlights the spectral purity issue. Plotted in this figure is the net count rate versus wavelength of BD+28D4211 observed with E140M at central wavelength 1425 Å. The wavelength region around Lyman- α is extracted from $m = 36$. Lyman- α is a black line in BD+28D4211 and should be at the zero level, independent of the extraction height. The actual net spectrum is overcorrected at Lyman- α , with the overcorrection increasing with larger extraction height.

Figure 2 compares the gross, net, and background count rates of BD+28D4211 for a fixed extraction height of 7 pixels. Figure 2a is the region around Lyman- α . The fitted background spectrum amounts to about 25% of the peak rate of the gross spectrum and is higher than the count rate in the Lyman- α core. The net count rate becomes negative in the Lyman- α line core. The principal source for the overcorrection is scattered light, which becomes even more important for larger extraction height (dotted line for $h = 11$ in Figure 2a). Lyman- α bottoms out at -0.5 counts/s/p for $h = 11$, while the $h = 7$ extraction improves by 40% to -0.3 counts/s/p.

The effects of scattered light are far less important for E230H. In Figure 2b we show the gross, net, and background count rates of BD+75D325 observed in the E230H mode for an extraction height of 7 pixels. The spectral region is around the Mg II doublet. The structure of Figure 2b is the same as 2a. The background shows no wavelength dependence and is small in comparison with the gross spectrum. The black Mg II lines are properly at 0 level after the background correction.

A small extraction height minimizes the uncertainty in the background correction. In the future, post-processing software will become available to correct for the over-subtraction of the background due to scattered light.

4. Photometric Precision

Although not the first priority for most echelle observers, photometric precision is a consideration for choosing the optimum extraction height. Figure 3 shows the net count rates of BD+28D4211 for extraction heights of 3, 5, 7, 9, 11, 15, and 21 pixels. The rates

are normalized by dividing by the values measured through the 11 pixels extraction aperture. Three modes and wavelength/order combinations are selected for inclusion in panels a), b), and c) to illustrate the typical behavior. Heights larger than 5 pixels result in throughputs of at least 90%, except at the extreme wavelengths for each order. The 21-pixel height extracts close to 100% of the source flux. However, the spectra extracted with $h = 3$ and 5 pixels have significant quasi-periodic noise.

The results in Figure 3 argue in favor of an extraction height of at least 5 pixels.

5. Signal-to-noise versus Extraction Height for Continuum Sources

The signal-to-noise initially increases with extraction height, as more target flux is extracted. After a critical height is reached, the signal-to-noise decreases, as more and more noise from the background is added. In Figure 4 we show the signal-to-noise versus extraction height for representative gratings and wavelengths. In each figure, the results for all orders of a particular grating and central wavelength combination are plotted after averaging over the central 200 pixels in the dispersion direction. The signal-to-noise values are normalized to the peak value in each order.

As expected, a turn-over of the maximum signal-to-noise is seen. The location of the turn-over depends on the target signal relative to the background. In all studied cases, most of the background is due to scattered light, which is stronger at shorter than at longer wavelengths. Therefore, the drop-off in the signal-to-noise with h is more pronounced for the E140 modes and for the shortest wavelengths of each mode.

The behavior of the curves in Figure 4 is independent of the target flux, as long as the dark noise is negligible. In the absence of dark noise, the background is predominantly due to scattered light, which is approximately a constant fraction of the source flux at each wavelength.

The simulations demonstrate that extraction heights between 5 and 11 pixels retain at least 98% of the maximum signal-to-noise at all wavelengths for all modes.

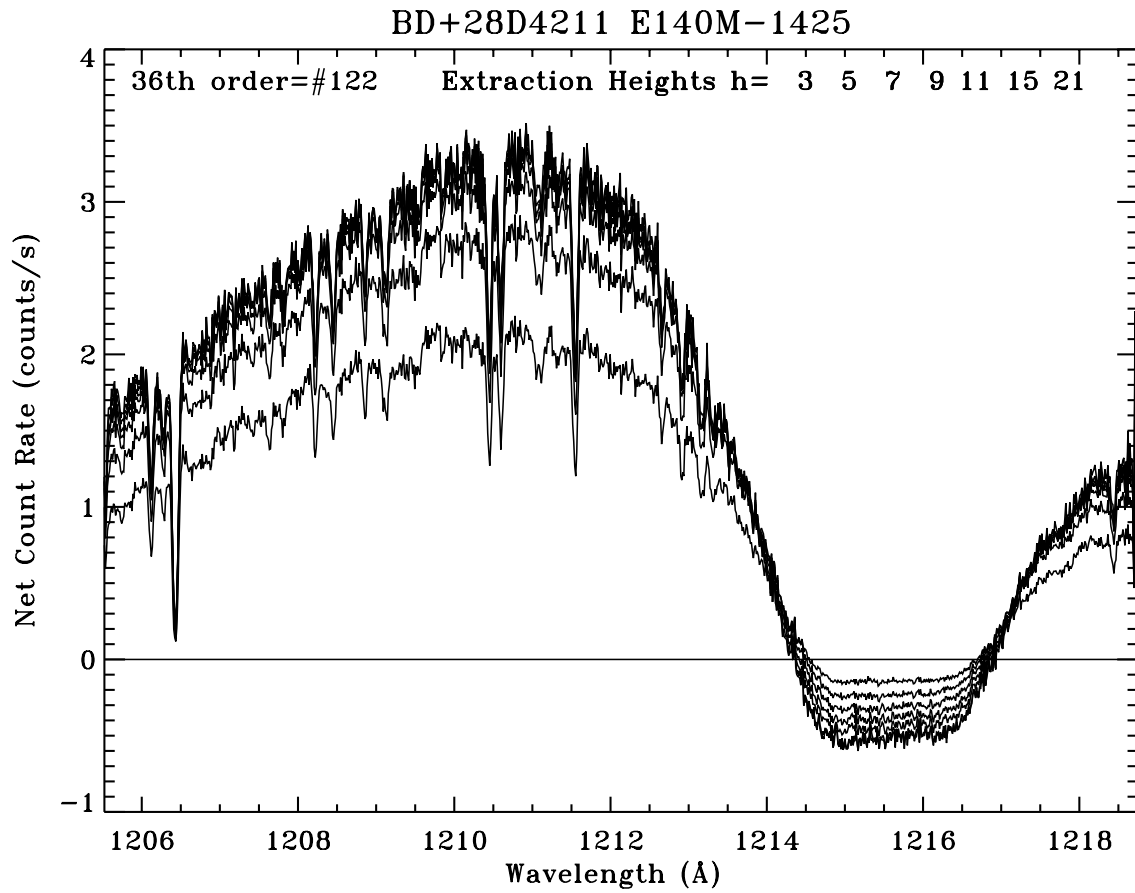
6. Recommendations.

The optimum extraction height for STIS echelle spectra of point sources depends on the amount of scattered light, the desired photometric precision, and the signal-to-noise. There is no height that would optimize all constraints simultaneously. Since our goal is to define a height that would fit most needs, and at the same time has as few variables as possible, our selection is guided by the requirement to maximize photometric precision and spectral purity. A height of 7 pixels for all echelle modes is acceptable as the default for point source extractions. An extraction height of 7 pixels is very close to the extraction height which maximizes the signal-to-noise for all modes and encompasses more than

98% of the target flux. The STScI pipeline will use $h = 7$ pixels for echelle extractions. GOs will be able to extract spectra for different heights with the **x1d** STSDAS task.

7. Figures

Figure 1: Net count rate versus wavelength of BD+28D4211 observed with E140M at central wavelength 1425 Å ($m = 122$). The seven spectra plotted are extracted with heights of 3, 5, 7, 9, 11, 15, and 21 pixels. Larger extraction heights have larger count rates at the peak (1211 Å) and more negative rates in the Lyman- α absorption line.



LEITHERER: pitech 11-Mar-1998 17:47

Figure 2: **a)** Gross, net, and background count rate of BD+28D4211 around Lyman- α . The net count rate (spectrum reaching about 3 counts/s at 1211 Å) is obtained after subtracting the background (smooth curve peaking at about 1.3 counts/s) from the gross spectrum (top spectrum) for an extraction height of 7 pixels. For comparison, an extraction height of 11 pixels (dotted curve) gives an even stronger overcorrection of the Lyman- α absorption. **b)** Gross, net, and background count rate of BD+75D325 around the Mg II doublet. As in a), the net, gross, and background are shown for an extraction height of 7 pixels. At this wavelength the background is small; and the gross and net differ by a few percent only. The Mg II lines in the net spectrum are black, as expected.

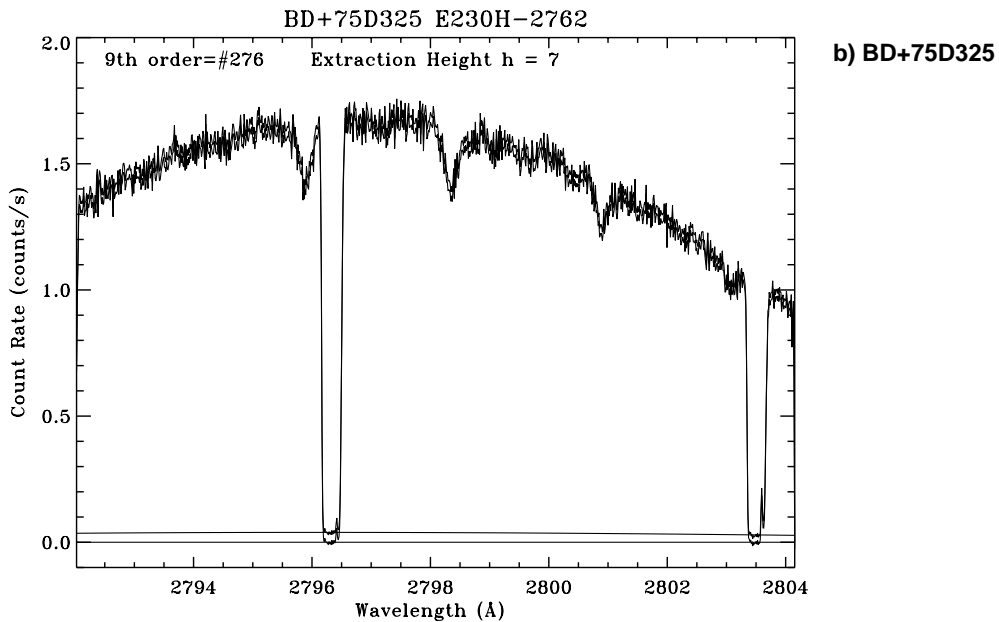
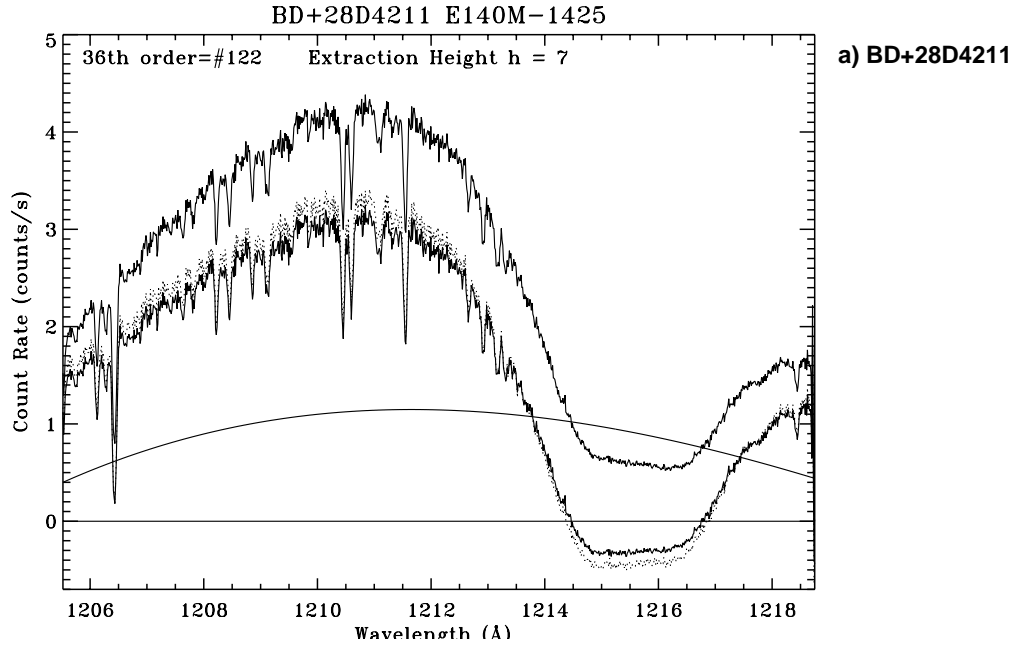
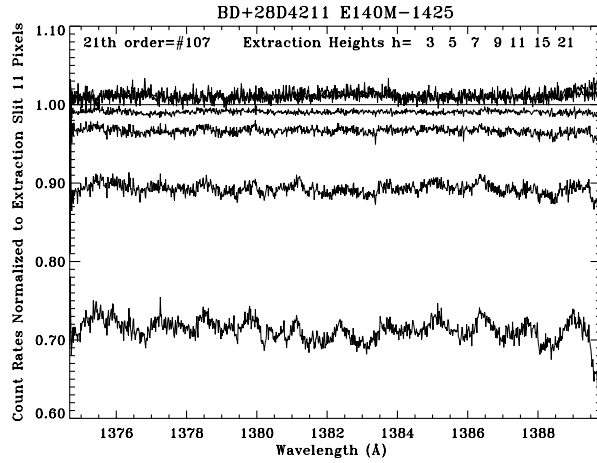
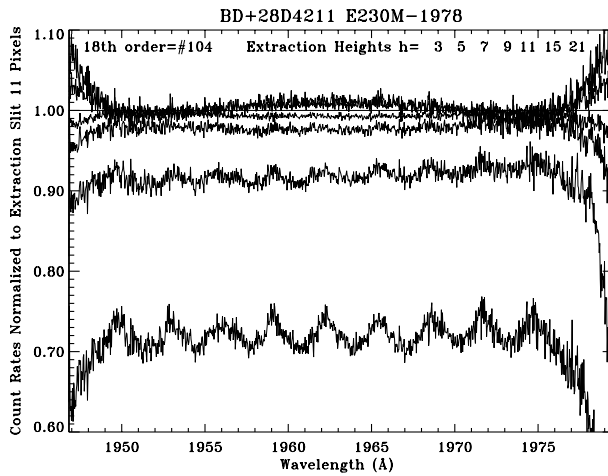


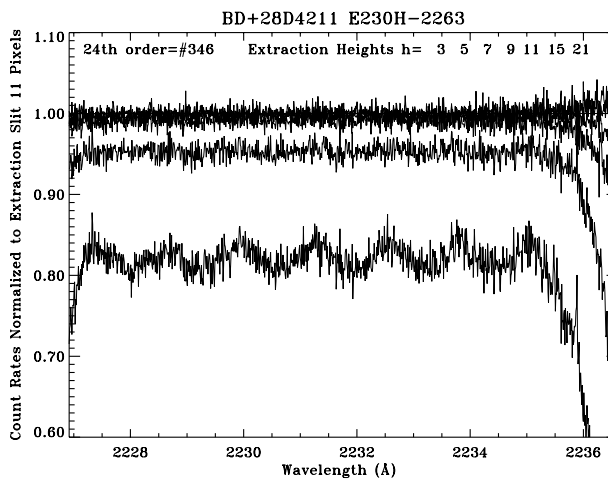
Figure 3: Net count rates of BD+28D4211 for extraction heights of 3, 5, 7, 9, 11, 15, and 21 pixels. The rates are normalized by dividing by the values measured with the 11 pixels extraction height. **a)** Results for $m = 107$ of E140M around 1380 Å. **b)** Results for $m = 104$ of E230M around 1960 Å. **c)** Results for $m = 346$ of E230H around 2230 Å.



a) $m=107$, E140M, 1380Å



b) $m=104$, E230M, 1960Å



c) $m=346$, E230H, 2230Å

Figure 4: Signal-to-noise versus extraction height for representative gratings and wavelengths. Each figure contains the results for all orders of a particular grating and central wavelength combination. All signal-to-noise values are normalized to the peak value found for each order. **a)** Results for BD+28D4211 and E140M at 1425 Å. **b)** BD+28D4211 and E230M at 1978 Å. **c)** BD+28D4211 and E230M at 2707 Å. **d)** BD+75D325 and E140H at 1234 Å. **e)** BD+75D325 and E140H at 1416 Å. **f)** BD+75D325 and E140H at 1598 Å. **g)** BD+75D325 and E230H at 2013 Å. **h)** BD+75D325 and E230H at 2762 Å. **i)** BD+75D325 and E230H at 3012 Å.

